

Estimation and reduction of random noise in mass anomaly time-series from satellite gravity data by minimization of month-to-month year-to-year double differences

Ditmar, Pavel; Tangdamrongsub, Natthachet; Ran, Jiangjun; Klees, Roland

DOI

[10.1016/j.jog.2018.05.003](https://doi.org/10.1016/j.jog.2018.05.003)

Publication date

2018

Document Version

Accepted author manuscript

Published in

Journal of Geodynamics

Citation (APA)

Ditmar, P., Tangdamrongsub, N., Ran, J., & Klees, R. (2018). Estimation and reduction of random noise in mass anomaly time-series from satellite gravity data by minimization of month-to-month year-to-year double differences. *Journal of Geodynamics*, 119, 9-22. <https://doi.org/10.1016/j.jog.2018.05.003>

Important note

To cite this publication, please use the final published version (if applicable).
Please check the document version above.

Copyright

Other than for strictly personal use, it is not permitted to download, forward or distribute the text or part of it, without the consent of the author(s) and/or copyright holder(s), unless the work is under an open content license such as Creative Commons.

Takedown policy

Please contact us and provide details if you believe this document breaches copyrights.
We will remove access to the work immediately and investigate your claim.

Estimation and reduction of random noise in mass anomaly time-series from satellite gravity data by minimization of month-to-month year-to-year double differences

Pavel Ditmar, Natthachet Tangdamrongsub¹, Jiangjun Ran^{2,*}, Roland Klees*

Delft University of Technology, Stevinweg 1, 2628 CN, Delft, The Netherlands

Abstract

We propose a technique to regularize a GRACE-based mass-anomaly time-series in order to (i) to quantify the Standard Deviation (SD) of random noise in the data, and (ii) to reduce the level of that noise. The proposed regularization functional minimizes the Month-to-month Year-to-year Double Differences (MYDD) of mass anomalies. As such, it does not introduce any bias in the linear trend and the annual component, two of the most common features in GRACE-based mass anomaly time-series. In the context of hydrological and ice sheet studies, the proposed regularization functional can be interpreted as an assumption about the stationarity of climatological conditions. The optimal regularization parameter and noise SD are obtained using Variance Component Estimation. To demonstrate the performance of the proposed technique, we apply it to both synthetic and real data. In the latter case, two geographic areas are considered: the Tonlé Sap basin in Cambodia and Greenland. We show that random noise in the data can be efficiently (1.5 – 2 times) mitigated in this way, whereas no noticeable bias is introduced. We also discuss various findings that can be made on the basis of the estimated noise SD. We show, among others, that knowledge of noise SD facilitates the analysis of differences between GRACE-based and alternative estimates of mass variations. Moreover, inaccuracies in the latter can also be quantified in this way. For instance, we find that noise in the surface mass anomalies in Greenland estimated using the Regional Climate Model RACMO2.3 is at the level of 2 – 6 cm equivalent water heights. Furthermore, we find that this noise shows a clear correlation with the amplitude of annual mass variations: it is lowest in the north-west of Greenland and largest in the south. We attribute this noise to limitations in the modelling of the meltwater accumulation and run-off.

Keywords: Mass transport, GRACE, Tikhonov regularization, Variance Component Estimation, Tonlé Sap, Greenland Ice Sheet

*Corresponding author

Email address: jiangjunrangmail.com (J. Ran)

¹Currently at: University of Newcastle, Australia

²Currently at: State Key Laboratory of Geodesy and Earth's Dynamics, Institute of Geodesy and Geophysics, Chinese Academy of Sciences, Wuhan, China

Preprint submitted to Journal of Geodynamics

May 14, 2018

1. Introduction

The Earth's system is characterized by on-going large-scale mass transport. In most of land areas, it is associated with various hydrological processes. An exception are the polar regions, where the dominant contributors are ice sheets and Glacial Isostatic Adjustment (GIA).

An accurate quantification of large-scale mass-transport is of major importance in various applications, including water management, climate science, and solid Earth geophysics. Satellite Gravimetry (SG) is a powerful tool to monitor large-scale mass transport. The first satellite mission suitable for that purpose – Gravity Recovery and Climate Experiment (GRACE) – was launched in 2002 (Tapley et al., 2004). In the first instance, SG data are used to compute time-series of the Earth's gravity field solutions. Typically, one solution per month is obtained. Each of them consists of a set of spherical harmonic coefficients complete to some maximum degree (usually between 60 and 120). After appropriate processing (see, e.g., Wahr et al., 1998; Ditmar, 2018), such solutions may yield a time-series of mass anomalies within a region of interest, i.e., the differences between the instantaneous amount of mass at (or near) the Earth's surface and the corresponding long-term mean value. Currently, the GRACE mission is not operational anymore, but its successor – GRACE Follow-On (GFO) – is scheduled for launch in early 2018 (Flechtner et al., 2014, <https://gracefo.jpl.nasa.gov>).

Mass anomalies extracted from SG data suffer from inaccuracies. A part of the error budget consists of random noise propagated from the original satellite observations via spherical harmonic coefficients. Such noise is not time-correlated and may be quite strong, especially if the target region is small. The estimated mass anomalies may suffer also from systematic disturbances. For instance, various filters are typically used to reduce noise in spherical harmonic coefficients (Wahr et al., 1998; Han et al., 2005; Wouters and Schrama, 2007; Swenson and Wahr, 2006; Kusche, 2007; Klees et al., 2008; Siemes et al., 2013). Unfortunately, filters also distort the signal of interest, introducing among others leakage errors.

The random and systematic errors mentioned above may complicate the usage of SG-based mass anomaly estimates in practice. For instance, these errors make it more problematic to estimate the quality of a geophysical model describing mass transport of a certain type when SG is used as a source of independent information. This is because the differences between the geophysical model and SG-based estimates will be contaminated by errors in the latter estimates themselves. This may be particularly harmful if errors in SG-based estimates are comparable to or exceed errors in the geophysical model.

With this article, we present a novel procedure that allows for: (i) quantifying the level of random noise in a mass anomaly time-series based on SG data; and (ii) reducing this level. The basic properties of the proposed procedure are as follows:

- It is based on the Tikhonov regularization concept (Tikhonov and Arsenin, 1977) and does not require an explicit parameterization of the signal in the time domain, which makes the procedure very flexible
- A new variant of the regularization functional is proposed, which minimizes the month-to-month year-to-year double differences in order to keep seasonal variations and linear trends (the dominant features of many mass transport processes) untouched, so that the bias introduced by the regularization is reduced.
- Known stochastic properties of random noise (e.g., time-dependent standard deviation or full error variance-covariance matrix) can be accounted for in the statistically optimal way

- The optimal regularization parameter is computed by Variance Component Estimation (VCE) (Koch and Kusche, 2002), which makes the procedure not only flexible, but also fully automatized.
- VCE allows also for a re-estimation of the random noise level in the original SG-based estimates.

The ability of the procedure to quantify the level of random noise in a mass anomaly time-series from the time-series itself makes it particularly valuable when SG is used for the validation of a geophysical model. Knowledge of this level allows for a quantification of the contribution of random noise in SG-based estimates to their differences with respect to the time-series subject to validation. Then, it is easy to estimate the Standard Deviation (SD) of remaining noise, which is composed of systematic errors in SG estimates and noise in the geophysical model assuming that remaining noise is not correlated with random noise in SG estimates. This opens the door for the quantification of noise in the geophysical model alone (since the contribution of systematic errors in SG estimates can be assessed by, e.g., a numerical experiment).

The proposed procedure has been already successfully used in a number of studies: to assess the performance of a novel variant of a so-called mascon approach in the context of Greenland Ice Sheet monitoring with SG (Ran et al., 2017); to calibrate the error covariance matrices of degree-1 and C_{20} spherical harmonic coefficients estimated from a combination of GRACE-based monthly solutions and an ocean bottom pressure model (Sun et al., 2017); as well as to demonstrate the added value of a novel technique for GRACE data processing by considering the estimated mass anomalies in Mississippi River basin and in Greenland (Guo et al., 2018). In this article, we present an in-depth analysis of the proposed techniques, including an open discussion of its strong points and limitations. We focus on two geographical areas as representative examples. The first one is the Tonlé Sap basin (Cambodia), which is subject to large seasonal and inter-annual mass variations of hydrological origin. The other area is Greenland, where a combination of snow fall and ice mass loss results in strong seasonal mass variations combined with large negative long-term trends. The two examples were deliberately chosen to demonstrate that the proposed methodology has a broad spectrum of potential applications. Among others, we discuss how the aforementioned "remaining noise" can be quantified and how this information can be used to know more about a mass anomaly time-series alternative to the SG-based one. In addition, we isolate the "remaining noise" in the differences between *regularized* SG estimates and the alternative time-series. This allows us to quantify the level of random noise in SG estimates after regularization and, therefore, to assess how efficiently that noise is damped by the proposed procedure.

The structure of the article is as follows. Sect. 2 contains a description of the proposed regularization procedure. In Sect. 3, we apply the developed procedure to mass anomaly time-series based on simulated and real GRACE data. Among others, we discuss in detail how the SD of "remaining noise" and the reduction of random noise by regularization can be quantified (Sect. 3.1.2). Furthermore, realistic numerical simulations are conducted in order to support real data processing and make a comprehensive assessment of performance of the proposed regularization scheme. Sect. 4 contains a discussion and conclusions.

2. Theory

Mass anomaly time-series $H_i^{(\text{obs})}$ based on SG data may contain gaps and strong noise. The proposed technique allows for a quantification and reduction of the noise level, as well as for fill-

ing in data gaps, if they are present. To that end, the Tikhonov regularization concept (Tikhonov and Arsenin, 1977) is used. To simplify the presentation of the method, we assume that the regularized mass anomaly time-series is a continuous function $\hat{H}(t)$, where t is time in years. The corresponding equations for discrete time-series are provided in Appendix A. In the actual implementation of the proposed technique, the discretization of the original and regularized time-series is always one month.

We postulate that the regularized time-series $\hat{H}(t)$ minimizes the penalty functional

$$\Phi[H] = \sum_i \left(H(t_i) - H_i^{(\text{obs})} \right)^2 + \alpha \Omega[H], \quad (1)$$

where t_i is the time of the i -th observation, α is the regularization parameter, and $\Omega[H]$ is the regularization functional. The latter depends on the function $H(t)$ and its derivatives up to a given order. For simplicity, we assume here that noise in the input data is white. A generalization to arbitrary Gaussian noise is straightforward (see Appendix A).

The highest order of the derivatives of $H(t)$ used in the definition of the regularization functional defines the order of that functional. A commonly-used Tikhonov regularization functional is the zero-order functional

$$\Omega[H] = \int (H(t))^2 dt, \quad (2)$$

which requires that the target function $\hat{H}(t)$ is as close to zero as possible. As an alternative, the first-order functional

$$\Omega[H] = \int (H'(t))^2 dt \quad (3)$$

(where $H'(t)$ is the time-derivative of $H(t)$) is used frequently. This functional tries to make the unknown function the smoothest possible one. In the context of GRACE data processing, a somewhat similar idea was applied in the computation of mascon solutions (see, e.g., Luthcke et al., 2006, 2013). Both zero- and first-order functionals inevitably bias the solution, since they penalize all signals (an exception is a constant, which is not penalized by the first-order functional). This makes their application to mass anomaly time series sub-optimal.

Many mass anomaly time-series typically show a pronounced annual periodicity; the temporal behaviour of mass anomalies in neighboring years is rather similar. This applies to, e.g., most signals of hydrological origin, as well as to signals related to the part of an ice sheet that is subject to summer melt. Therefore, we believe that a regularization functional that takes this periodicity into account would be a more natural choice when estimating mass anomalies. The most straightforward way to design such a regularization functional is to minimize the year-to-year differences of mass anomalies:

$$\Omega[H] = \sum_{k=1}^{K-1} \int_0^1 (h_{k+1}(t) - h_k(t))^2 dt, \quad (4)$$

where K is the total number of years considered and $h_k(t)$ is by definition the mass anomaly in the k -th year ($t \in [0; 1]$; $h_k(1) = h_{k+1}(0)$ due to the continuity of $H(t)$; we remind that t is time in years).

Unfortunately, the regularization functional of Eq. (4) penalizes an inter-annual variability of mass anomalies. This is a weak point whenever such a variability is present. This holds true, for

instance, for many hydrological processes (particularly, in areas where a long-term depletion of groundwater stocks takes place), as well as for ice sheets and mountain glaciers, many of which are subject to a long-term mass loss nowadays. Furthermore, a GIA-related signal may also be responsible for inter-annual mass variations (namely, long-term nearly-linear trends). Therefore, we propose to minimize the year-to-year difference not between mass anomalies themselves but between their time-derivatives:

$$\Omega[H] = \sum_{k=1}^{K-1} \int_0^1 (h'_{k+1}(t) - h'_k(t))^2 dt. \quad (5)$$

After discretization, this reduces to a minimization of Month-to-month Year-to-year Double Differences (MYDD). Obviously, such a functional does not penalize year-to-year differences in the presence of an arbitrary (but constant) offset between mass anomalies in neighbouring years. The regularization functional of Eq. (5) is exploited here.

In the context of hydrological and ice sheet studies, the regularization functional of Eq. (5) has a physical interpretation. According to the mass balance equation, the rate of mass change in a particular river basin or ice drainage system is equal to the difference between mass gain (i.e., precipitation) and mass loss (e.g., due to evaporation, transpiration, sublimation, water run-off, or ice discharge). Thus, the proposed regularization functional of Eq. (5) does not penalize the mass anomaly signals that reflect stationary climatological conditions (i.e., when the mass gains and mass losses per calendar month do not change from year to year).

To find the optimal regularization parameter α , we propose to use Variance Component Estimation (VCE). A brief description of this method, adapted from (Koch and Kusche, 2002), is provided in Appendix A. An advantage of VCE is that it not only provides the optimal regularization parameter, but also allows the level of noise in the input data to be quantified.

To illustrate the behaviour of the regularization functional of Eq. (5), we consider a simple numerical example. Let the true time-series $H(t)$ covering a 3-year time interval be analytically defined as

$$H(t) = A \sin 2\pi t + Ct, \quad t \in [0; 3], \quad (6)$$

where $A = 1$ cm in terms of Equivalent Water Height (EWH) and $C = 0.5$ cm/yr, see Fig. 1. Furthermore, the observations are assumed to be noise-free and cover only the first and the second year of the considered time interval, where the sampling rate is one month. The adopted regularization scheme allows the full 3-year time-series of mass anomalies to be restored. Since the seasonal variability of the considered function does not change, the proposed regularization scheme fully recovers it on the basis of the available data, without introducing any bias (Fig. 1). In particular, the linear trend is fully recovered, which is due to the fact that the requirement of similarity in successive years is applied to the time-derivatives of mass anomalies rather than to mass anomalies themselves.

It can be proven analytically that any function $H(t)$ not penalized by the regularization functional of Eq. (5) is a combination of arbitrary seasonal variations and a linear trend (see Appendix B). This means that the class of functions that can be processed with the proposed regularization without suffering from a bias is relatively wide. This may also have a negative effect. If a time-series is too short or noise is too strong, the regularized time-series may contain pronounced periodic features that are purely noise-driven and do not represent a real signal. To illustrate this, we consider a true function $H(t)$, which comprises only a linear trend over a 3-year time interval:

$$H(t) = Ct, \quad t \in [0; 3], \quad (7)$$

Fig.
1

where $C = 0.5$ cm/yr (EWH). The observations simulated with a one-month sampling rate cover the entire time interval. They are artificially contaminated with a relatively strong white noise of 1-cm EWH standard deviation (Fig. 2, top plot). By chance, the simulated observations in November of each year suffer from a positive noise value. As a result, the regularized time-series shows a strong peak in this month. It is worth adding that the VCE estimate of the data noise SD remains reasonable: 1.020 cm EWH. Thus, the estimation error is only 2%.

Next, we repeat the previous experiment, using a two-times longer set of synthetic observations: six years instead of three. All the other parameters of the experiment are kept as before. In that case, the regularized time-series still suffers from data noise, but its impact is dramatically reduced (Fig. 2, bottom plot). Remarkably, the VCE estimate of the noise SD of 0.988 cm EWH is even more accurate than in the previous experiment. This differs from the actual noise SD by only 1.2%.

Fig.
2

3. Application

In this section, we apply the proposed regularization procedure to mass anomaly time-series in two geographical areas: (i) the Tonlé Sap basin in Cambodia and (ii) Greenland. In both cases, the processed time-series are based on real GRACE data. In Sect. 3.1, we provide general information about the GRACE data, and the data analysis approach (particularly, about quantifying the reduction of random noise in GRACE data after regularization). In Sections 3.2 and 3.3, we present the results for the Tonlé Sap basin and Greenland, respectively. The structure of both sections is similar. First, we discuss the data processing aspects specific for the considered geographical area. Second, we discuss the results of a numerical study, where the behaviour of actual mass anomalies is reproduced. Third, we consider the results of real data processing.

3.1. General information

3.1.1. Input data

The space segment of the GRACE mission consisted of two twin satellites, which followed each other in a nearly the same polar orbit with a 200-km separation. The satellites were equipped, among others, with a K-Band Ranging (KBR) system, which allowed temporal variations in the inter-satellite separation to be measured with micrometer-level precision. A number of research centres process GRACE observations to produce a time-series of monthly gravity field solutions, which form the core of the so-called level-2 data product of the GRACE mission. In our study, we make use of the solutions produced at the Center for Space Research (University of Texas at Austin) (Bettadpur, 2012). Each of these solutions is formed by a set of spherical harmonic coefficients complete either to degree 60 (this variant was used to estimate mass anomalies over the Tonlé Sap basin) or to degree 96 (this variant was used for Greenland). Degree-1 coefficients are absent in the GRACE level-2 data product. Therefore, an independently computed time-series of these coefficients (Swenson et al., 2008) was exploited. Furthermore, the spherical harmonic coefficient $C_{2,0}$ was replaced in each GRACE monthly solution by the one estimated from satellite ranging data (Cheng and Tapley, 2004) due to an insufficient accuracy of the former one.

Mass anomaly estimates based on GRACE data are contaminated by random noise. The noise level increases rapidly with decreasing size of the area of interest. This noise is not correlated in the time domain, but shows a strong spatial correlation, which reflects, among others, the anisotropic sensitivity of GRACE KBR observations. They sense the along-track (North-South)

component of the mass anomaly gradient much better than the cross-track (East-West) component. As such, random noise in mass anomaly estimates depends also on the shape of the area of interest: an area elongated in the East-West direction is a much more favourable study object than an area elongated in the North-South direction. In addition, random noise increases towards the equator due to a lower density of satellite groundtracks, as well as due to small intersection angles of ascending and descending tracks, which makes the sensitivity of measurements particularly anisotropic. State-of-the-art data processing in the spatial domain was applied to produce mass anomaly estimates with the lowest possible noise level. Further details are provided in sections 3.2.1 (Tonlé Sap basin) and 3.3.1 (Greenland).

3.1.2. Analysis of results

For both study areas, GRACE-based mass anomaly time-series are compared with reference ones, which are obtained with other techniques. The points of our special attention are: (i) quantification of random noise in GRACE data; (ii) the bias introduced into the data by the proposed regularization procedure; and (iii) reduction of noise in GRACE data after regularization. In a simulated experiment, an estimation of the noise SD after regularization is straightforward. In an experiment with real data, a reference dataset is needed. Doing so, we follow a two-step procedure. In the first step, we analyse the difference between the original GRACE data set (i.e., the data set not subject to any interpolation or regularization) and the reference one. These differences reflect (i) random noise in GRACE data and (ii) "other" errors, which may include inaccuracies of the reference data, as well as systematic errors in GRACE data (for instance, those due to signal leakage). We assume that random noise and "other" errors are not cross-correlated, so that

$$\Delta_{\text{orig}}^2 = \sigma_{\text{GRACE-orig}}^2 + \sigma_{\text{other}}^2, \quad (8)$$

where Δ_{orig} is the rms difference between GRACE and reference data, $\sigma_{\text{GRACE-orig}}$ is the SD of random noise in the original GRACE data (which is estimated using VCE) and σ_{other} is the SD of the other errors. This allows the SD of "other" errors to be estimated as

$$\sigma_{\text{other}} = \sqrt{\Delta_{\text{orig}}^2 - \sigma_{\text{GRACE-orig}}^2}. \quad (9)$$

In the second step, we analyze the difference between the regularized GRACE data and the reference data. Assuming that the effect of regularization on the systematic errors in GRACE data is negligible, we can state that

$$\Delta_{\text{reg}}^2 = \sigma_{\text{GRACE-reg}}^2 + \sigma_{\text{other}}^2, \quad (10)$$

where Δ_{reg} is the rms difference between the two data sets and $\sigma_{\text{GRACE-reg}}$ is the SD of random noise in the regularized GRACE data. Eq. (10) allows the latter noise to be quantified as

$$\sigma_{\text{GRACE-reg}} = \sqrt{\Delta_{\text{reg}}^2 - \sigma_{\text{other}}^2}. \quad (11)$$

We use the quantity

$$\frac{\sigma_{\text{GRACE-reg}}}{\sigma_{\text{GRACE-orig}}} \times 100\% \quad (12)$$

to describe the reduction of random noise in a particular GRACE dataset due to regularization. Finally, knowledge of "other" errors imposes an upper limit for possible errors in the reference data and in systematic errors in GRACE data. If there are reasons to believe that the contribution of the latter errors is minor, the estimate σ_{other} can be used to quantify the accuracy of the reference data themselves.

3.2. Tonlé Sap basin

Tonlé Sap basin located in Cambodia has an area of $82 \times 10^3 \text{ km}^2$. It surrounds the Tonlé Sap Lake, which is the largest freshwater lake in Southeast Asia. The region is characterized by monsoon climate, the rainy season lasting from May to September or early October. As a result, a flood event takes place in the second half of each year, usually reaching the peak in October.

3.2.1. Data preparation

In this study, we use two time-series of mass anomalies over the Tonlé Sap basin: a GRACE-based and a reference one. Both time-series were prepared by one of the co-authors and exploited earlier in (Tangdamrongsub et al., 2016).

The time-series of GRACE-based mass anomalies is based on monthly gravity field solutions pre-processed as explained in Sect. 3.1.1. At the next step, the solutions were cleaned from along-track artefacts by means of the de-stripping procedure (Swenson and Wahr, 2006) and smoothed with a Gaussian filter of 350-km half-width (Jekeli, 1981; Wahr et al., 1998). After that, the smoothing effect of the Gaussian filter was mitigated by a signal restoration technique (Chen et al., 2014). Finally, the (unregularized) time-series of monthly mass anomalies within the Tonlé Sap basin was computed (Wahr et al., 1998). Mass anomalies in the months without GRACE data were obtained by means of a cubic polynomial interpolation, using the Matlab function *interp1*. Further details regarding the adopted data processing scheme can be found in (Tangdamrongsub et al., 2016).

The reference estimates of mass anomalies in Tonlé Sap basin were obtained on the basis of surface reflectance data collected by the Moderate-Resolution Imaging Spectroradiometer (MODIS) instrument on board Terra and Aqua satellites (Vermote et al., 2011). The reflectance data were used to estimate the mean inundated area within the Tonlé Sap basin in each month. A comparison of those estimates with GRACE-based mass anomalies allowed an empirical relationship between the two time-series to be established:

$$H(x, t) = a_0 + a_1 x(t) + a_2 e^{-\frac{x(t)}{1000}} + a_3 \cos 2\pi t + a_4 \sin 2\pi t, \quad (13)$$

where t is time in years (zero time being at the beginning of a year), $H(t)$ is mean mass anomaly within the basin in cm EWH, x is inundated area in km^2 , and a_0, \dots, a_4 are constant coefficients obtained by means of the linear regression: $a_0 = -0.54$, $a_1 = 1.4 \times 10^{-3}$, $a_2 = -16.2$, $a_3 = -4.8$, and $a_4 = -9.2$. The last two terms in Eq. (13) were needed to take into account seasonal variations in the soil moisture content (Tangdamrongsub et al., 2016).

In our study presented below, we use as input unregularized mass anomaly estimates in the time-interval (Jan. 2003 – Oct. 2014). To improve the consistency between the GRACE- and MODIS-based mass anomalies, we have estimated their mean values in the considered time interval (the months with no GRACE data being excluded in both cases). After that, the corresponding mean value has been subtracted from each data set. The resulting GRACE- and MODIS-based time-series can be seen in Fig. 3 as blue dots and red lines, respectively. They both show a clear seasonal variability, with the maximum in October. In the first half of the considered time interval (i.e., 2003 – 2008), about the same annual pattern is visible with a peak amplitude in the range 25 – 30 cm EWH. In the second half of the considered time interval (2009 – 2014), a strong inter-annual variability is observed. In odd years (2009, 2011, and 2013), the peak mass anomaly reaches 40 cm EWH, which is substantially above the average peak level observed in 2003 – 2008. In even years (2010, 2012, and 2014), the peak anomaly reaches only about 20 cm. Such an inter-annual variability poses a challenge for the proposed procedure, since the latter is tailored to scenarios when seasonal variations in neighbouring years are similar.

286 3.2.2. Numerical study

287 The time-series of mass anomalies in the Tonlé Sap basin is mimicked by a quasi-periodic
 288 function $H(t)$ that reaches minimum and maximum in April and October of each year, respec-
 289 tively. In 2003 – 2008, the signal amplitude stays at the same middle level A_m . In 2009–2014, the
 290 signal amplitude is year-dependent: it stays at a high level A_h in odd years and at a low level A_l
 291 in even years. More specifically:

$$H(t) = c + A[1 - \cos(2\pi t - \varphi)], \quad (14)$$

292 where

$$A = \begin{cases} A_m & \text{in Jan.2003–Mar.2009,} \\ A_h & \text{in Apr.2009–Mar.2010,} \\ & \text{Apr.2011–Mar.2012,} \\ & \text{Apr.2013–Mar.2014;} \\ A_l & \text{in Apr.2010–Mar.2011,} \\ & \text{Apr.2012–Mar.2013,} \\ & \text{Apr.2014–Oct.2014.} \end{cases} \quad (15)$$

293 The phase φ is set equal to 1.8326, which corresponds to the mid of April (the month when
 294 the mass anomalies are the lowest). The numerical values of the coefficients c , A_m , A_h , and
 295 A_l are estimated from the mass anomalies based on real GRACE data with a linear regression:
 296 $c = -21.42$ cm; $A_m = 20.53$ cm; $A_h = 27.28$ cm; and $A_l = 17.31$ cm. The simulated time-
 297 series is contaminated by pseudo-random zero-mean Gaussian white noise with a SD of 4.2 cm,
 298 which is consistent with our estimation of noise in real data processing (see Sect. 3.2.3). To
 299 make the results more representative, each numerical experiment is repeated with 1000 different
 300 noise realizations. The major outcome of each experiment is: (i) an estimate of the noise SD in
 301 the original data time-series; (ii) the noise SD after regularization; and (iii) the bias introduced
 302 by regularization. Noise after regularization is defined as the difference between the regularized
 303 noisy time-series and the true one. It is a combination of regularized random noise and the
 304 bias of the true signal introduced by regularization. To quantify the latter, we re-estimate the
 305 signal amplitudes from the regularized time-series with the linear regression, and then subtract
 306 the true amplitudes. For each estimate, we report the mean over the 1000 realizations and the
 307 corresponding SD.

308 In the first experiment, the time interval 2003 – 2008 is considered. In this time interval, the
 309 true signal is exactly periodic, which is an ideal case for the proposed regularization procedure.
 310 In this experiment, the estimate of the random noise SD is very close to the true value, whereas
 311 the bias introduced by the regularization is negligible (Table 1). The reduction of data noise is
 312 quite substantial: the noise SD after regularization is only 44% of the original one.

313 In the second experiment, we consider the time interval 2009 – 2014, when the true signal
 314 shows a substantial inter-annual variability. As a result, the SD of noise in the original data is
 315 estimated less accurately (in average, it is under-estimated by about 15%: see Table 1). Further-
 316 more, a moderate bias is introduced (about 5% of the difference between the high amplitude A_h
 317 and the low amplitude A_l). The noise reduction due to regularization is still substantial (though
 318 more modest than in the first experiment): the SD of noise after regularization is 73% of the
 319 original one.

320 The third experiment covers the entire time interval 2003 – 2014. In this experiment, the be-
 321 havior of the signal component that does not follow the annual periodicity (and, therefore, is

*Table
1*

penalized by regularization) is different over the years: it is absent in the first half of the considered time interval and relatively large in the second half. As a result, regularization introduces a bias into the A_h and A_l signal amplitudes, which is larger than in the second experiment: in average, about 14% of the difference $A_h - A_l$ (see Table 1). On the other hand, the noise SD of the original data is estimated much more accurately than in the second experiment: in average, it is underestimated by only 2%. We see two factors that may lead to that improvement. First, it is a longer duration of the considered time-series, which makes the VCE procedure more robust (there is a less chance that a part of random noise shows a periodic behaviour and, therefore, escapes the quantification; see also the discussion at the end of Sect. 2). Second, it is the absence of a non-annual signal in the first half of the considered time interval. As a result, at least half of the considered data set offers the ideal conditions for the quantification of random noise. To separate the contribution of these two factors, we conduct another numerical experiment.

The time interval considered in the fourth experiment is the same as in the third one: 2003 – 2014. The true signal, however, experiences inter-annual variations over the entire time interval, i.e., the expression Eq. (15) describing the signal amplitude is modified as follows:

$$A = \begin{cases} A_h & \text{in Apr.2003–Mar.2004,} \\ & \text{Apr.2005–Mar.2012,} \\ & \text{Apr.2007–Mar.2008,} \\ & \text{Apr.2009–Mar.2010,} \\ & \text{Apr.2011–Mar.2012,} \\ & \text{Apr.2013–Mar.2014;} \\ A_l & \text{in Jan.2003–Mar.2003,} \\ & \text{Apr.2004–Mar.2005,} \\ & \text{Apr.2006–Mar.2007,} \\ & \text{Apr.2008–Mar.2009,} \\ & \text{Apr.2010–Mar.2011,} \\ & \text{Apr.2012–Mar.2013,} \\ & \text{Apr.2014–Oct.2014.} \end{cases} \quad (16)$$

It turns out that now, the noise SD is estimated more accurately than in the second experiment: the under-estimation is reduced from 15% to 10% (Table 1). Still, this estimate is much less accurate than the one obtained in the third experiment. This means that the accurate estimation of the noise SD in the third experiment is mostly explained by the absence of an inter-annual signal in 2003 – 2008.

Finally, we note that the level of random noise in all the numerical experiments presented so far is relatively high: 4.2 cm EWH or 42% of the difference between the high amplitude A_h and the low amplitude A_l . One may ask how the performance of the proposed procedure depends on the signal-to-noise ratio. In order to shed light on this issue, we conduct the fifth numerical experiment. It is identical to the third one, but the noise SD is reduced from 4.2 to 2.0 cm. The reduction of the noise level makes its estimation with the proposed procedure more difficult: the resulting estimate is, in average, about 20% lower than the actual noise level (see Table 1). Furthermore, the reduction of the noise level due to regularization is more modest than in any of the previous experiments: the resulting noise SD is 77% of the original one. On the other hand, the bias is lower than before: less than 3% of the difference $A_h - A_l$.

3.2.3. Regularization of mass anomalies based on real GRACE data

Here, we use the time-series of GRACE-based mass anomalies excluding the months when original GRACE data do not exist (that is, the results produced by interpolation are ignored). In line with the findings of the numerical study, the obtained results look satisfactory, including the time interval 2009 – 2014 (black lines in Fig. 3). A closer inspection still reveals some bias introduced by the regularization: the peak values in the year of extreme flood events (2009, 2011, and 2013) become smaller, whereas the peak value in the dry year 2010 becomes larger. This effect is, however, minor. At the same time, regularization clearly reduces random noise in the original GRACE-based estimates.

The statistics related to GRACE and reference mass anomaly estimates, as well as to their differences, is summarized in column 3 of Table 2. Just like in the numerical study, we also split the entire time interval under consideration into two sub-intervals: (I) 2003 – 2008 and (II) 2009 – 2014. Table 2 reports the results both for the individual sub-intervals and for the total interval (I+II).

The rms difference between the GRACE (non-regularized) and reference mass anomalies is about 6 cm EWH, the results for sub-intervals I and II being very similar. At the first glance, this could be interpreted as an evidence of a similar accuracy of the time-series within the entire time interval under consideration. A further analysis shows, however, that this is not the case. VCE reveals that the noise SD of the un-regularized GRACE time-series changes in time substantially: it exceeds 5 cm EWH in the first sub-interval but drops more than two times in the second time interval. According to the findings of the numerical study, this difference can be partly explained by the presence of inter-annual signal variations in 2009 – 2014. In the case of real data, however, this difference is much larger. A discussion of this reduction in the estimated noise level is continued in Sect. 4.

The SD of "other" errors estimated with Eq. (9) also shows a temporal variability. Unlike random noise, "other" errors increase: from about 3 cm EWH to more than 5 cm EWH. We explain this by a limited performance of the empirical link given by Eq. (13), particularly when the behaviour of mass anomalies deviates from a "regular" behaviour. For instance, GRACE shows that extreme flood events, like those in 2011 and 2013, are followed by an increased mass level in the course of the next dry season, as compared to other years (Fig. 3). Most probably, this is because extreme flood events cause an accumulation of large ground water stocks, which are not fully depleted in the course of the next year. The reference data, which are based only on the extent of open water bodies, cannot observe this process.

Application of regularization reduced the contribution of GRACE to the differences between GRACE-based and reference mass anomalies. As a result, the dependence of the differences on time increases: the rms difference increases from 4.6 cm EWH in the first sub-interval to 5.5 cm EWH in the second one.

Finally, the noise SD after regularization is estimated with Eq. (11). It turns out that regularization reduces random noise rather substantially: to 60 – 66% of the original level. Remarkably, the reduction is similar for both sub-intervals and for the entire time interval under consideration. Furthermore, the result is consistent with the findings of the numerical study. All this increases the confidence in the results obtained.

3.3. Greenland

The area of Greenland exceeds 2 million km². Most of it is covered by the Greenland Ice Sheet (GrIS) – the second largest ice sheet on Earth. GrIS contains enough ice to rise global mean sea level by 7.4 m (Vaughan et al., 2013). The GrIS mass balance is primarily a sum of two components: the Surface Mass Balance (SMB) and ice discharge. The SMB reflects the relationship

Table 2

between the surface mass gain and mass loss processes, which are predominantly represented by snowfall and meltwater runoff, respectively (Van den Broeke et al., 2009). Seasonal GrIS mass variations are usually attributed to SMB only; the variations in ice discharge are believed to be slow (Van den Broeke et al., 2009). In our study, we rely on this assumption, in spite of recent evidences that ice discharge may contribute to the GrIS mass balance at inter-annual (Moon et al., 2012) and seasonal time scales (Moon et al., 2014). We address mass variations both over the entire Greenland and over individual drainage systems. In the latter case, the territory of Greenland is split into 5 regions: North (N), North-West (NW), North-East (NE), South-West (SW), and South-East (SE) (see Fig. 4), which is consistent with previous studies (e.g., Van den Broeke et al., 2009; Ran et al., 2017).

Fig.
4

3.3.1. Data preparation

Since a mass re-distribution caused by GIA is present in the study area, the model of A et al. (2013) was used to clean GRACE monthly sets of spherical harmonic coefficients from that signal. Next, each monthly solution was converted into a set of mass anomalies using the mascon approach of Ran (2017); Ran et al. (2017). This leads to a higher spatial resolution and reduced signal leakage, as compared to a direct conversion of spherical harmonic coefficients into mass anomalies. In particular, the signal leakage from Greenland to the surrounding ocean can be prevented, while preserving the in-land signal from damping. The lateral mass anomaly distribution within each mascon was assumed to be homogeneous. Importantly, the inversion of spherical harmonic coefficients into mass anomalies per mascon was performed without any filtering or regularization, in order to mitigate the signal leakage between the mascons. Of course, this could result in a higher noise level, as compared to a spatially-filtered or regularized solution. However, that noise can be mitigated by applying a regularization in the time domain, as is discussed below. The territory of Greenland was split into 28 mascons. The obtained mass anomalies (in Gt) were summed up to give the total mass anomaly per drainage system and for entire Greenland, respectively.

The set of reference mass anomalies was extracted from daily SMB estimates based on the Regional Atmospheric Climate Model, version 2.3 (RACMO 2.3) (Ettema et al., 2009). The original SMB estimates (in terms of EWH) were integrated over time and then averaged in space and time to produce the total mass anomaly per region per month. To restore the ice discharge signal, the differences between GRACE- and RACMO-based mass anomaly time-series were approximated by a quadratic algebraic polynomial. After that, those polynomials were added back to the corresponding RACMO-based time-series.

As an example, we present the obtained results for the NW drainage system and entire Greenland in Fig. 5. The unregularized GRACE-based time-series and RACMO-based time-series are shown there as blue dots and red lines, respectively. In the NW drainage system, seasonal mass variations are hardly visible. The dominant signal is a long-term negative trend, which increases in the course of time. As far as entire Greenland is concerned, an accelerated mass loss is also visible, but that long-term behaviour takes place in the presence of a clear seasonal cycle: mass accumulates in winter and diminishes in summer. Particular large mass loss is observed in the year 2012, which is notorious for an extensive summer melt over the entire GrIS (Nghiem et al., 2012).

Fig.
5

3.3.2. Numerical study

We use the time-series shown in Fig. 5 to set up two numerical experiments. In each experiment, we reproduce the behaviour of actual mass anomalies (represented in terms of EWH). As

444 in the numerical experiments discussed in Sect.3.2.2, the "true" signals are defined analytically
 445 and contaminated by pseudo-random zero-mean Gaussian white noise. The noise SD was de-
 446 fined consistently with the corresponding estimate based on real data (see Sect. 3.3.3). In each
 447 experiment, 1000 noisy time-series realizations are synthesized and analyzed.

448 In the first experiment, we reproduce mass changes in the NW drainage systems. The corre-
 449 sponding time-series is approximated by a parabola:

$$H(t) = \frac{a(t - t_0)^2}{2} + b(t - t_0) + c. \quad (17)$$

450 The reference time t_0 is in the middle of the considered time interval, i.e., the beginning of July
 451 2008. This is needed to avoid the absorption of the trend estimate b by the acceleration term in
 452 a linear regression analysis. The constant coefficients a , b , and c are defined on the basis of real
 453 GRACE-based time-series: $a = -1.82 \text{ cm/yr}^2$, $b = -16.29 \text{ cm/yr}$, and $c = -45.64 \text{ cm}$. The noise
 454 SD is set equal to 3.4 cm.

455 In this experiment, the proposed regularization procedure shows an excellent performance
 456 (Table 3). The SD of actual noise is only 3% below the true value, whereas the noise SD after
 457 regularization is reduced to the level of 38% of the original one. It is also remarkable that
 458 the bias introduced by regularization is negligible in both the trend estimate and the estimated
 459 acceleration. This is in spite of the fact that the acceleration term does not belong to the class
 460 of functions exempt from penalization. We explain this by the fact that the "local" impact of the
 461 acceleration term in each particular set of neighbouring months is minor, so that the simulated
 462 function is still close to the ideal one.

463 In the second numerical experiment, we mimic the behaviour of mass anomalies of entire
 464 Greenland. To that end, we extend the signal of Eq. (17) with an annual term:

Table
3

$$H(t) = \frac{a(t - t_0)^2}{2} + b(t - t_0) + c + A [1 - \cos(2\pi(t - t_0) - (\varphi - \varphi_0))]. \quad (18)$$

465 In line with the real mass anomaly time-series, the phase φ is set equal to 1.8326, which implies
 466 that the seasonal mass accumulation would reach a maximum in the middle of April if a long-
 467 term-trend were absent. The additional phase shift φ_0 is included to reflect the fact that the
 468 reference time t_0 does not coincide with the beginning of a year: $\varphi_0 = 2\pi(t_0 - \text{int}[t_0])$. The
 469 amplitude A of the annual signal is set equal to a certain "normal" level A_n in almost all the
 470 years. The only exception is the year 2012, when it is defined differently. More specifically:

$$A = \begin{cases} A_n & \text{in Jan.2003–Mar.2012,} \\ & \text{Apr.2013–Dec.2013;} \\ A_{2012} & \text{in Apr.2012–Mar.2013.} \end{cases} \quad (19)$$

471 All the constant coefficients are estimates by a linear regression from the real GRACE-based
 472 time-series shown in the bottom plot of Fig. 5: $a = -1.13 \text{ cm/yr}^2$, $b = -13.21 \text{ cm/yr}$, $c = -23.40$
 473 cm , $A_n = -8.57 \text{ cm}$, and $A_{2012} = -14.30 \text{ cm}$. The SD of the noise added to the synthetic signal
 474 is set equal to 1 cm, which makes the experiment set-up consistent with real data processing (see
 475 Sect. 3.3.3). Such a noise level is rather low. For instance, it is only 17.5% if the difference
 476 between the normal annual amplitude A_n and the annual amplitude in 2012 A_{2012} . In that sense,
 477 this set-up is close to the set-up of the fifth (low-noise) numerical experiment considered in
 478 Sect. 3.2.2.

479 The results obtained after applying regularization are, in general, better than those of the fifth
480 experiment in Sect. 3.2.2. The original noise SD is underestimated by only 10%, whereas the
481 noise SD after the regularization is reduced to the level of 69%, as compared to the original one
482 (Table 3). Furthermore, the biases introduced into the linear trend, acceleration, and the normal
483 annual signal amplitude are negligible. For instance, the bias in the annual signal amplitude does
484 not exceed, in average, 1% of the difference $A_n - A_{2012}$. A good performance of the regularization
485 procedure in this experiment is explained by the fact that the signal is close to the ideal one: the
486 annual signal stays most of the time at a constant level, whereas the impact of the acceleration
487 term apparently remains minor. On the other hand, it is worth noticing that the bias introduced
488 into the annual signal in 2012 reaches 8% of the difference $A_n - A_{2012}$. Though we still consider
489 such a bias as minor, it is definitely larger than those observed in the fifth (low-noise) numerical
490 experiment considered in Sect. 3.2.2. This is a clear indication that "unusual" signals (e.g., a
491 larger mass loss in a particular summer than in average) are subject to larger distortions. This is
492 an expected result, since the regularization tends to make such signals similar to the signals in
493 neighboring years.

494 3.3.3. Regularization of mass anomalies based on real GRACE data

495 Finally, we apply the proposed regularization procedure to mass anomalies extracted from real
496 GRACE data. As in Sect. 3.2.3, we split the considered time interval into two sub-intervals in or-
497 der to make the analysis more representative and to facilitate a consistency check of the results:
498 (I) 2003 – 2007 and (II) 2008 – 2013. The results both for the individual sub-intervals (I, II)
499 and for the total interval (I+II) are analyzed. In the latter case, two variants of the recovered ice
500 discharge signals are considered. In both variants, those signals are approximated by quadratic
501 polynomials, as explained above. The only difference is that in the first variant, a single poly-
502 nomial is computed for the entire time interval 2003 – 2013. We consider it as the "primary"
503 variant; it is used, in particular, to compute the reference mass anomalies shown in Fig. 5. In
504 the alternative variant, on the other hand, the best-fitting quadratic polynomials are found for the
505 sub-intervals 2003 – 2007 and 2008 – 2013 independently. Thus, the reference mass anomaly
506 time-series in the alternative variant is nothing but the result of merging the reference time-series
507 for sub-intervals (I) and (II). A comparison of the results of these two variants allows some con-
508 clusions to be drawn regarding their robustness with respect to long-term uncertainties associated
509 with ice discharge.

510 Regularized GRACE time-series for the NW drainage system and entire Greenland are shown
511 in Fig. 5 as black lines. In columns 4 – 7 of Table 2, we present further information about the
512 outcome of the regularization for the drainage systems N, NW, NE, and the combined region
513 "SW&SE". The last column reports the obtained results for entire Greenland.

514 The estimated SD of random noise in GRACE-based mass anomalies for the northern drainage
515 systems (N, NW, and NE) is quite similar: 3 – 4 cm EWH. This is in spite of the fact that the
516 area of the drainage system N is more than two times smaller than that of the other regions.
517 Most probably, this can be explained by the northern location of the drainage system N, so that
518 its small size is compensated by a high density of GRACE ground tracks. The region SW&SE
519 shows a relatively low noise level: 1 – 2.5 cm. We explain this by the shape of that region: unlike
520 the regions NW and NE, it is not extended in the meridional direction, which implies a higher
521 accuracy of GRACE-based mass anomaly estimates. The lowest noise level (0.8 – 0.9 cm) is
522 observed for entire Greenland, which is definitely due to the large size of this region. The noise
523 levels estimated for the entire time interval (I+II) and the sub-intervals (I) and (II) show a good
524 agreement. The only exception is the SW&SE region, where a substantial reduction in the noise

level is observed. As similar reduction was observed earlier in the analysis of mass anomalies in the Tonlé Sap basin (Sect. 3.2.3). This issue is further discussed in Sect. 4.

The rms differences between the non-regularized GRACE-based mass anomalies and the reference ones show less variability than the random errors in GRACE estimates discussed above: they stay at the level of 3 – 5 cm EWH, except for the southern region SW&SE, where the RMS difference reach 5 – 7 cm. In two cases (N and entire Greenland), the rms differences computed over the entire time interval (I+II) are larger than the errors computed for both sub-intervals I and II, if the first variant of ice discharge correction is exploited. When the alternative variant of ice discharge correction is applied (i.e., when the corresponding quadratic polynomials are estimated for the two sub-intervals individually), the rms differences obtained for the entire interval I+II are always between the rms differences obtained for the sub-intervals I and II, as expected.

By subtracting the contribution of random noise from the obtained rms differences in line with Eq. (9), we estimate the SD of "other" noise. "Other" noise for the entire GrIS likely reflects errors in the SMB estimates produced by the RACMO model, as well as the processes not related to the ice sheet surface, such as the meltwater retention inside the ice layer and the residual ice discharge signal. The contribution of a multi-year time-scale to "other" noise can be assessed by a comparison of the estimates obtained with the two variants of ice discharge correction in 2003 – 2013: 3.1 cm EWH for the first variant versus 2.6 cm EWH for the alternative one. Thus, the contribution of a multi-year time-scale is at the level of only 15%; the rest of "other noise" is likely associated with a relatively short time scale (2 – 3 years or less). "Other" noise estimates for individual drainage systems show a substantial variability. Those estimates, however, must be interpreted with some caution. The fact is, all of them are obtained by subtracting two close numbers. Thus, the observed variability may reflect inaccuracy of the obtained error estimates. An extreme example is the drainage system NE in time interval II. "Other" noise cannot be quantified in that case at all, since the rms difference between GRACE (original) and reference time-series is smaller than the estimated error SD of GRACE-based mass anomalies. However, in spite of these uncertainties, the "other" errors show a consistent behaviour. They stay at a mid level (2.5 – 3 cm EWH) for the drainage systems N and NE, as well as entire Greenland; they reduce to ~2 cm for the drainage system NW, and increase to 5 – 6 cm for the region SW&SE. This behavior shows an excellent correlation with the mean amplitude of annual signals in the considered regions: 7 – 9 cm EWH in the regions with the mid level of "other errors", ~4 cm in the drainage system NW with a low error level, and ~17 cm in the region SW&SE, where the level of "other" errors is relatively high (see the last row in Table 2). We believe, therefore, that the observed errors reveal deficiencies associated with modelling the summer ice melting (the primary cause of seasonal mass variability).

The rms differences between the regularized GRACE-based mass anomalies and the reference mass anomalies are also computed. Then, Eq. (11) allows us to quantify random noise in GRACE-based mass anomalies after regularization. It turns out that the regularization typically reduces the random noise SD to 40 – 60% of the original value. This outcome is an agreement with the results of the numerical studies. In a few cases, an even more substantial reduction of random noise seems to be achieved. For instance, the SD of random noise for entire Greenland is estimated for some time intervals as only ~ 20% of the original level. However, these estimates are likely caused by an underestimation of the original noise SD due to its low level, as it is discussed in Sect. 3.3.2. If, for instance, the true noise SD is originally equal to 1 cm (i.e., if this underestimation is 10%, which is not impossible according to the conducted numerical study), the estimate of noise SD after the regularization should be increased from ~20% to ~50% of the original level, which is consistent with the other results.

4. Discussion and conclusions

In this study, we developed a statistically-optimal regularization technique that allows one to smooth and interpolate a mass anomaly time-series based on satellite gravimetry data, as well as to estimate the level of random noise in it. The proposed regularization functional minimizes the MYDD (month-to-month year-to-year double differences) of mass anomalies. As we showed theoretically, this functional does not introduce any bias into two types of signals, which commonly occur in the Earth's system: arbitrary signals with an annual periodicity and long-term linear trends.

We conducted a number of numerical simulations, in which actual signals and errors in GRACE-based mass anomaly time-series were reproduced. In all the considered experiments, the bias introduced into the actual signals was minor and did not exceed, in average, 14%. The largest bias was observed in the cases when the level of random noise was high and when the signal in a given year was substantially different from the signal in the neighbouring years. At the same time, the developed regularization scheme effectively reduces random noise. In the considered numerical experiments, for instance, the noise SD was typically reduced to 40 – 70 % of the original level. The factors that facilitate an efficient noise reduction are high level of noise in the original time-series and minimal inter-annual variability of signals.

Another important outcome of the proposed regularization methodology is the assessment of random noise in mass anomaly time-series; such estimates are provided by the VCE procedure, which is a part of the regularization technique. Conducted numerical experiments showed that the obtained estimates of noise SD are close to the true values or slightly less. However, this under-estimation did not exceed 22% in the conducted experiments. The factors that facilitate an accurate estimation of noise SD are a long duration of the analyzed time-series and a relatively high noise level, as compared to the penalized signal (the signal that shows neither an annual periodicity nor a long-term linear behaviour).

The proposed technique can be considered as a handy tool to quantify the accuracy of various mass anomaly time-series in general. As such, it can be applied, for instance, to estimate the performance of a particular methodology designed for SG data processing, to compare the accuracy of alternative mass anomaly estimates, to demonstrate and compare the impact of various supporting data used in SG data processing, etc. Examples of such applications can already be found in (Sun et al., 2017; Ran et al., 2017; Guo et al., 2018).

In our study, we applied the developed procedure to analyze GRACE-based time-series of mass anomalies in the Tonlé Sap basin in Cambodia and Greenland. In this way, we showed how some more findings can be extracted from the estimates of random noise SDs.

First, the noise SD estimates allow for a separation of the contribution of random noise and "other" errors when GRACE mass anomalies are compared with mass anomalies derived from other data and/or models. The "other" errors comprise systematic errors in GRACE data (e.g., due to signal leakage) and errors in the reference data. In the study of Greenland, for instance, we found that the SD of "other" errors stays at the level of 2 – 6 cm EWH and strongly correlates with the amplitude of the annual signal. From this, we concluded that the revealed errors are likely associated with modelling of summer ice melting. The most probable cause of these errors is meltwater accumulation and run-off. On the one hand, the signal related to meltwater may be quite significant, since it takes meltwater, in average, about two weeks to leave GrIS (van Angelen et al., 2014). On the other hand, this signal is not fully taken into account by the RACMO2.3 model: it implies that the run-off process is instantaneous. A further analysis of this signal in GRACE-based mass anomalies can be found in (Ran, 2017). Speaking more generally,

the conducted study opens the door for a more accurate quantification of noise in reference mass anomalies when the latter are compared with those based on SG data. This concerns any application area of SG, such as the study of ice sheets, hydrology, oceanography, and others.

Second, the quantification of "other" errors allowed us to estimate the SD of random noise in GRACE-based mass anomalies after regularization. It turned out that regularization typically reduces noise to 40 – 66% of the original level (i.e., about 1.5 – 2 times). This is in a good agreement with the results of numerical experiments.

A division of the considered time interval into two allowed us to check the internal consistency of the noise SD estimates obtained for a given region. The estimates obtained for entire Greenland and for its northern regions turned out to be in a reasonable agreement (the differences were within 20%, cf. Table 2). However, the estimates obtained for the combined SW&SE region of Greenland and for the Tonlé Sap basin turned out to be quite different: they show that noise in 2009 – 2014 or 2008 – 2013 is noticeably (more than 2 times) lower than in 2003 – 2008 or 2003 – 2008. To shed more light on this issue, we considered, among others, the SW and SE regions of Greenland separately. For the SE region (the area is 398,000 km²), the obtained estimates of noise SD were 9.2 cm, 8.3 cm, and 9.3 cm for the time intervals (I), (II), and (I+II), respectively. For the small SW region (the area is 214,000 km²), the corresponding estimates were 18.0 cm, 14.3 cm, and 16.6 cm, respectively. Thus, even though some noise reduction is observed, it stays with the 20-% limit. From this and other evidences, we conclude that a very large reduction in the noise level observed for the the combined SW&SE region of Greenland and the Tonlé Sap Basin is likely an evidence of an insufficient robustness of the proposed technique when short (≤ 6 years) are concerned. Thus, it is advised to consider results obtained for such time intervals with a caution.

Another caveat concerns the temporal behaviour of the signals in the time-series under consideration. The proposed regularization functional minimizes a variant of signal double-differences, which implies that the signal must change smoothly in the time domain. Obviously, a signal that rapidly change from month to month may be over-regularized, whereas the level of random noise may be overestimated. In the extreme case, when the stochastic behavior of signal is not distinguishable from that of white noise, the separation of the time-series into signal and noise is, naturally, impossible.

It is also worth mentioning that the proposed regularization technique may be used to fill in gaps in mass anomaly time-series. Since the year 2011, the GRACE data time-series suffers from multiple gaps, which are frequently filled in by means of interpolation. We found, however, that the obtained results are not necessarily better than those produced with a simple interpolation scheme (e.g., cubic splines). A typical example in the estimation of mass anomalies for entire Greenland in August-September 2013, when no GRACE data were available (see the inset in the bottom plot in Fig. 5). Unfortunately, this is exactly the time interval when rapid mass loss due to summer melting occurred. By chance, a particularly large summer mass loss took place one year earlier – in 2012. Then, the proposed regularization technique uses that mass change pattern to fill in the gap in 2013. However, the RACMO model shows that mass loss in summer 2013 was minor. Then, a cubic interpolation, which ignores the behaviour of mass anomalies in other years, apparently yields better results. This illustrates a conceptual problem associated with data gaps. The presence of such gaps means some loss of information in the collected data. If the behavior of a target process in that time interval is "non-typical" in whatever sense, a reliable recovery of such behavior becomes conceptually impossible: no mathematical technique can replace a collection of field measurements.

The proposed regularization technique has space for further improvements. For instance, we

assumed so far that noise in the mass anomaly time-series is stationary. In reality, this may not be the case because the accuracy of GRACE-based mass anomalies may change in time. There are several reasons for that. First, the altitude of GRACE satellites rapidly decreased after year 2011 (http://www2.csr.utexas.edu/grace/operations/orbit_evolution/semiB.png), which must have had a positive impact on the accuracy and spatial resolution of the mass anomaly estimates; Second, the attitude control of GRACE satellites was relatively poor at the beginning of the mission, which may reduce the quality of the resulting estimates (Inácio et al., 2015). Third, GRACE orbits enter the periods of a short repeat cycle from time to time, which also deteriorates the quality of the resulting estimates (Wagner et al., 2006). In addition, switching from GRACE to GFO data in the future will also likely change the accuracy of mass anomaly estimates due to a higher accuracy of the onboard instruments. Finally, it is not unlikely that gaps in GRACE time-series, as well as the gap between the GRACE and GFO missions will be somewhat filled in by the usage of GNSS data from various other satellite missions. Though the accuracy of GNSS data is relatively low, still they definitely can capture some mass transport signals (Ditmar et al., 2009; Gunter et al., 2011; Weigelt et al., 2013; Guo et al., 2017). Thus, the picture of future mass anomaly time-series will not be "black-and-white" (mass anomaly is either provided or not provided). Instead, the time-series will likely be continuous, but of rather heterogeneous quality: more accurate in the months when GRACE or/and GFO data are available and much less accurate otherwise. As it is shown in Appendix A, the proposed regularization technique can be easily adjusted to such a situation. Then, this technique may become a tool to homogenize future mass anomaly time-series by exploiting all available information in the statistically optimal sense (i.e., taking into account the accuracy of each particular monthly estimate).

Another direction of further developments is the optimal estimation of the regularization parameter, taking into account the dependence of the actual mass anomaly signal on time. Currently, the adopted regularization procedure makes use of time-invariant soft constraints (cf. Eqs. (A.3-A.5) in Appendix A). In reality, the expected deviations of the actual signal from a regular behaviour may show a variability in time (an example is the mass anomalies in the Tonlé Sap basin in 2009 – 2014). By taking this variability into account in the construction of the regularization functional, one may further improve the quality of the regularization.

Acknowledgements

The authors thank the Center for Space Research at the University of Texas at Austin for providing GRACE Level-2 data and the corresponding error variance-covariance matrices. The time-series of degree-1 spherical harmonic coefficients computed with the methodology of Swenson et al. (2008) was downloaded from the GRACE TELLUS website (ftp://podaac.jpl.nasa.gov/allData/tellus/L2/degree_1/). The SLR-based time-series of $C_{2,0}$ coefficients was downloaded from webpage ftp://ftp.csr.utexas.edu/pub/slr/geocenter/GCN_RL05.txt. The MODIS-based mass anomalies over the Tonlé Sap basin were derived from the MYD09A1 product, downloaded from <https://e4ftl01.cr.usgs.gov/MOLA/MYD09A1.005>. Furthermore, the authors thank B. Noël and M. van den Broeke from the Institute for Marine and Atmospheric Research (IMAU) of Utrecht University for providing SMB time-series over GrIS based on their RACMO 2.3 model. N. Tangdamrongsub thanks The Netherlands Organization for Scientific Research, NWO, for a financial support [project number 620 842.00.006]. J. Ran thanks his sponsor, the Chinese Scholarship Council. J. Ran was also partly supported by the Major National Scientific Research Plan [grant 2013CB733305] and the National Natural Science Foundation of China

[grants 41474063, 41674006, and 41431070]. In addition, the work was sponsored by the Stichting Nationale Computerfaciliteiten (National Computing Facilities Foundation, NCF) for the use of supercomputer facilities, with financial support from the Nederlandse organisatie voor Wetenschappelijk Onderzoek (Netherlands Organization for Scientific Research, NWO) [project SH-053]. Finally, the authors thank two anonymous reviewers for their numerous suggestions, which resulted in a substantial improvement of the manuscript.

References

- A, G., Wahr, J., Zhong, S., 2013. Computations of the viscoelastic response of a 3-D compressible Earth to surface loading: An application to glacial isostatic adjustment in Antarctica and Canada. *Geophysical Journal International* 192 (2), 557–572.
- Bettadpur, S. V., 2012. Gravity Recovery and Climate Experiment, UTCSR level-2 processing standards document for level-2 product release 0005. GRACE 327-742 (CSR-GR-12-xx). Center for Space Research, University of Texas at Austin.
- Chen, J., Li, J., Zhang, Z., Ni, S., 2014. Along-term groundwater variations in Northwest India from satellite gravity measurements. *Global and Planetary Change* 116, 130–138, doi:10.1016/j.gloplacha.2014.02.007.
- Cheng, M., Tapley, B., 2004. Variations in the Earth's oblateness during the past 28 years. *Journal of Geophysical Research B: Solid Earth* 109 (9), B09402 1–9.
- Ditmar, P., 2018. Conversion of time-varying Stokes coefficients into mass anomalies at the Earth's surface considering the Earth's oblateness. *Journal of Geodesy*.doi: 10.1007/s00190-018-1128-0.
- Ditmar, P., Bezdek, A., Liu, X., Zhao, Q., 2009. On a feasibility of modeling temporal gravity field variations from orbits of non-dedicated satellites. In: *International Association of Geodesy Symposia*. Vol. 133. pp. 307–313.
- Ettema, J., van den Broeke, M. R., van Meijgaard, E., van de Berg, W. J., Bamber, J. L., Box, J. E., Bales, R. C., 2009. Higher surface mass balance of the Greenland ice sheet revealed by high-resolution climate modeling. *Geophysical Research Letters* 36, L12501, doi: 10.1029/2009GL038110.
- Flechtner, F., Morton, P., Watkins, M., Webb, F., 2014. Status of the GRACE Follow-On mission. In: *International Association of Geodesy Symposia*. Vol. 141. pp. 117–121.
- Gunter, B., Encarnacao, J., Ditmar, P., Klees, R., 2011. Using satellite constellations for improved determination of Earth's time-variable gravity. *Journal of Spacecraft and Rockets* 48 (2), 368–377.
- Guo, X., Ditmar, P., Zhao, Q., Klees, R., Farahani, H., 2017. Earth's gravity field modelling based on satellite accelerations derived from onboard GPS phase measurements. *Journal of Geodesy* 91 (9), 1049–1068.
- Guo, X., Zhao, Q., Ditmar, P., Sun, Y., Liu, J., 2018. Improvements in the monthly gravity field solutions through modeling the colored noise in the grace data. *Journal of Geophysical Research: Solid Earth* (submitted).
- Han, S.-C., Shum, C. K., Jekeli, C., Alsdorf, D., 2005. Improved estimation of terrestrial water storage changes from GRACE. *Geophysical Research Letters* 32, L07302, doi: 10.1029/2005GL022382.
- Inácio, P., Ditmar, P., Klees, R., Farahani, H., 2015. Analysis of star camera errors in GRACE data and their impact on monthly gravity field models. *Journal of Geodesy* 89 (6), 551–571.
- Jekeli, C., 1981. Alternative methods to smooth the Earth's gravity field. Report No.327, Geodetic and GeoInformation Science. Department of Civil and Environmental Engineering and Geodetic Science, The Ohio State University.
- Klees, R., Rervtova, E. A., Gunter, B., Ditmar, P., Oudman, E., Winsemius, H. C., Savanije, H. H., 2008. The design of an optimal filter for monthly GRACE gravity field models. *Geophysical Journal International* 175, 417–432.
- Koch, K.-R., Kusche, J., 2002. Regularization of geopotential determination from satellite data by variance components. *Journal of Geodesy* 76, 259–268.
- Kusche, J., 2007. Approximate decorrelation and non-isotropic smoothing of time-variable grace-type gravity field models. *Journal of Geodesy* 81, 733–749.
- Luthcke, S., Sabaka, T., Loomis, B., Arendt, A., McCarthy, J., Camp, J., 2013. Antarctica, Greenland and Gulf of Alaska land-ice evolution from an iterated GRACE global mascon solution. *Journal of Glaciology* 59 (216), 613–631.
- Luthcke, S. B., Zwally, H. J., Abdalati, W., Rowlands, D. D., Ray, R. D., Nerem, R. S., Lemoine, F. G., McCarthy, J. J., Chinn, D. S., 2006. Recent Greenland ice mass loss by drainage system from satellite gravity observations. *Science* 314 (5803), 1286–1289.
- Moon, T., Joughin, I., Smith, B., Howat, I., 2012. 21st-century evolution of Greenland outlet glacier velocities. *Science* 336, 576–578, doi: 10.1126/science.1219985.
- Moon, T., Joughin, I., Smith, B., Van Den Broeke, M., Van De Berg, W., Noël, B., Usher, M., 2014. Distinct patterns of seasonal Greenland glacier velocity. *Geophysical Research Letters* 41 (20), 7209–7216.

763 Nghiem, S., Hall, D., Mote, T., Tedesco, M., Albert, M., Keegan, K., Shuman, C., DiGirolamo, N., Neumann, G.,
764 2012. The extreme melt across the Greenland Ice Sheet in 2012. *Geophysical Research Letters* 39 (20), L20502, doi:
765 10.1029/2012GL053611.

766 Ran, J., 2017. Analysis of mass variations in Greenland by a novel variant of the mascon approach, Ph.D thesis. Delft
767 University of Technology.

768 Ran, J., Ditmar, P., Klees, R., Farahani, H. H., 2017. Statistically optimal estimation of Greenland Ice Sheet mass
769 variations from GRACE monthly solutions using an improved mascon approach. *Journal of Geodesy*. 92, 299–319,
770 doi: 10.1007/s00190-017-1063-5.

771 Siemes, C., Ditmar, P., Riva, R. E. M., Slobbe, D. C., Liu, X. L., Farahani, H. H., 2013. Estimation of mass change trends
772 in the Earth's system on the basis of GRACE satellite data, with application to Greenland. *Journal of Geodesy* 87,
773 69–87, doi: 10.1007/s00190-012-0580-5.

774 Sun, Y., Ditmar, P., Riva, R., 2017. Statistically optimal estimation of degree-1 and C_{20} coefficients based on GRACE
775 data and an ocean bottom pressure model. *Geophysical Journal International* 210 (3), 1305–1322.

776 Swenson, S., Chambers, D., Wahr, J., 2008. Estimating geocenter variations from a combination of GRACE and ocean
777 model output. *Journal of Geophysical Research: Solid Earth* 113 (8), B08410, doi: 10.1029/2007JB005338.

778 Swenson, S., Wahr, J., 2006. Post-processing removal of correlated errors in GRACE data. *Geophysical Research Letters*
779 33, L08402, doi: 10.1029/2005GL025285.

780 Tangdamrongsub, N., Ditmar, P. G., Steele-Dunne, S. C., Gunter, B. C., Sutanudjaja, E. H., 2016. Assessing water re-
781 sources and exploring flood events over Tonlé Sap basin in Cambodia using GRACE and MODIS satellite observations
782 combined with hydrological models. *Remote Sensing of Environment* 181, 162–173.

783 Tapley, B. D., Bettadpur, S., Ries, J. C., Thompson, P. F., Watkins, M. M., 2004. GRACE measurements of mass variability
784 in the Earth system. *Science* 294, 2342–2345.

785 Tikhonov, A. N., Arsenin, V. Y., 1977. Solutions of ill-posed problems. V.H.Winston and Sons, Washington.

786 van Angelen, J., van den Broeke, M., Wouters, B., Lenaerts, J., 2014. Contemporary (1960–2012) evolution of the climate
787 and surface mass balance of the Greenland Ice Sheet. *Surveys in Geophysics* 35 (5), 1155–1174.

788 Van den Broeke, M., Bamber, J., Ettema, J., Rignot, E., Schrama, E., van de Berg, W. J., van Meijgaard, E., Velicogna,
789 I., Wouters, B., 2009. Partitioning recent Greenland mass loss. *Science* 326, 984–986.

790 Vaughan, D. G., Comiso, J. C., Allison, I., Carrasco, J., Kaser, G., Kwok, R., Mote, P., Murray, T., Paul, F., Ren,
791 J., Rignot, E., Solomina, O., Steffen, K., Zhang, T., 2013. Observations: Cryosphere. In: Stocker, T. F., Qin, D.,
792 Plattner, G.-K., Tignor, M., Allen, S. K., Boschung, J., Nauels, A., Xia, Y., Bex, V., Midgley, P. M. (Eds.), *Climate*
793 *Change 2013: The Physical Science Basis. Contribution of Working Group I to the Fifth Assessment Report of the*
794 *Intergovernmental Panel on Climate Change*. Cambridge University Press, Cambridge, United Kingdom and New
795 York, NY, USA.

796 Vermote, E. F., Kotchenova, S. Y., Ray, J. P., 2011. MODIS surface reflectance user's guide version 1.3. Technical report.
797 http://modis-sr.ltdri.org/guide/MOD09_UserGuide_v1_3.pdf.

798 Wagner, C., Mcadoo, D., Klokočník, J., Kostecký, J., 2006. Degradation of geopotential recovery from short repeat-
799 cycle orbits: Application to GRACE monthly fields. *Journal of Geodesy* 80 (2), 94–103.

800 Wahr, J., Molenaar, M., Bryan, F., 1998. Time variability of the Earth's gravity field: Hydrological and oceanic effects
801 and their possible detection using GRACE. *Journal of Geophysical Research* 103 (B12), 30,205–30,229.

802 Weigelt, M., Van Dam, T., Jggi, A., Prange, L., Tourian, M., Keller, W., Sneeuw, N., 2013. Time-variable gravity signal in
803 Greenland revealed by high-low satellite-to-satellite tracking. *Journal of Geophysical Research: Solid Earth* 118 (7),
804 3848–3859.

805 Wouters, B., Schrama, E. J. O., 2007. Improved accuracy of GRACE gravity solutions through empirical orthogonal
806 function filtering of spherical harmonics. *Geophysical Research Letters* 34, L23711, doi: 10.1029/2007GL032098.

Table 1: Results of the numerical study that reproduces mass variations over the Tonlé Sap Basin. The following information is provided for each of the experiments: (1) Considered time interval; (2) Reference to the analytic expression used to define the "true" signal; (3) Actual SD of pseudo-random noise added to the synthetic signal; (4) Noise SD estimated with the VCE technique; (5) Actual noise SD after the regularization; (6) Same as the previous item but in percentages of the original noise SD; and (7-9) Bias introduced by the regularization into the signal amplitudes. The shown error bars reflect the variability of the obtained estimates after the consideration of 1000 different noise realizations. Units are cm EWH.

Experiment	1	2	3	4	5
Time interval	2003–2008	2009–2014	2003–2014	2003–2014	2003–2014
True signal	Eq. (15)	Eq. (15)	Eq. (15)	Eq. (16)	Eq. (15)
Random noise SD before regularization (true)	4.20	4.20	4.20	4.20	2.00
Random noise SD before regularization (VCE-based estimation)	4.16±0.19	3.57±0.54	4.10±0.38	3.76±0.69	1.57±0.20
Noise SD after regularization	1.83±0.32	3.07±0.30	2.70±0.30	2.90±0.35	1.53±0.10
Noise after regularization (% of original noise)	44±8	73±7	64±7	69±8	77±5
Bias in the middle-amplitude signal (A_m)	0.01±0.70	N/A	0.08±0.58	N/A	0.01±0.27
Bias in the high-amplitude signal (A_h)	N/A	-0.53±0.88	-1.44±0.95	-0.68±0.63	-0.29±0.37
Bias in the low-amplitude signal (A_l)	N/A	0.49±0.87	1.36±0.88	0.69±0.63	0.26±0.35

Table 2: Results of two case studies (over the Tonlé Sap Basin and over Greenland) based on real data. In the second case, the results are shown both for individual drainage systems (columns "N" – "SE&SW") and for entire Greenland. The following estimates are provided for each of the considered regions: (1) SD of random noise in the original GRACE-based mass anomalies (i.e., before regularization), estimated with the VCE technique; (2) the rms difference between the GRACE-based (original) and reference mass anomalies; (3) SD of "other" errors (consisting of systematic errors in GRACE-based mass anomalies and errors in reference data); (4) the rms difference between the GRACE (regularized) and reference mass anomalies; (5) SD of random noise in GRACE-based mass anomalies after regularization; (6) same as the previous item but in percentages of the original random noise SD. The results are shown both for the individual sub-intervals (I and II) and the entire time interval (I+II). In the Tonlé Sap Basin case study, the sub-intervals are: (I) 01.2003 – 12.2008 and (II) 01.2009 – 10.2014. In the study of Greenland, the sub-intervals are: (I) 01.2003 – 12.2007 and (II) 01.2008 – 12.2013. Bold font is used for the estimates based on the time-series for the entire time interval (I+II) when the primary variant of ice discharge correction is exploited (i.e., when the RACMO-based time-series are corrected for ice discharge in the entire time interval at once). Italic font is used for the estimates based on the time-series for the entire time interval (I+II) and the alternative variant of ice discharge correction (i.e., when the RACMO-based time-series are corrected for ice discharge in the sub-intervals (I) and (II) individually). The last line shows the amplitude of annual variations in 2003 – 2013 in different Greenland regions estimated on the basis of the original GRACE data. Units are cm EWH.

	Time interval	Tonlé Sap basin	Greenland regions				
			N	NW	NE	SW & SE	Entire Greenland
Area (km ² × 10 ³) ^a		82	256	686	601	612	2154
1. Random noise in GRACE-based mass anomalies before regularization (VCE-based)	I+II	4.16	3.61	3.34	3.42	1.89	0.880
	I	5.42	3.44	3.60	3.81	2.48	0.802
	II	2.57	3.42	2.85	3.89	0.90	0.869
2. RMS difference from reference data before regularization	I+II	6.05	4.69	3.93	4.52	6.62	3.215
	I+II ^b	-	4.52	3.75	4.40	5.22	2.785
	I	6.25	4.40	4.02	5.12	5.30	2.834
	II	5.81	4.62	3.49	3.64	5.15	2.741
3. "Other" noise, including noise in reference data	I+II	4.40	2.99	2.08	2.95	6.34	3.093
	I+II ^b	-	2.72	1.72	2.76	4.86	2.642
	I	3.12	2.74	1.78	3.42	4.68	2.718
	II	5.22	3.11	2.02	-	5.07	2.599
4. RMS difference from reference data after regularization	I+II	5.06	3.55	2.71	3.32	6.38	3.096
	I+II ^b	-	3.35	2.49	3.14	4.92	2.650
	I	4.60	3.44	2.57	3.89	4.85	2.751
	II	5.48	3.56	2.64	2.91	5.07	2.607
5. Random noise in GRACE-based mass anomalies after regularization	I+II	2.50	1.91	1.74	1.51	0.72	0.151
	I+II ^b	-	1.97	1.80	1.49	0.77	0.199
	I	3.39	2.08	1.84	1.84	1.28	0.427
	II	1.68	1.74	1.70	-	0.29	0.203
6. Random noise in GRACE-base mass anomalies after regularization (% of original noise)	I+II	60%	53%	52%	44%	38%	17%
	I+II ^b	-	54%	54%	44%	41%	23%
	I	62%	60%	51%	48%	52%	53%
	II	66%	51%	60%	-	32%	23%
Amplitude of annual mass variations			7.6	3.8	7.5	17.4	9.0

^a – Shown areas reflect the geometry of regions used in GRACE data inversion (see Fig. 4). Those areas may somewhat deviate from the actual area of Greenland or the areas of individual drainage systems.

^b - The alternative variant of ice discharge correction is applied.

Table 3: Results of the numerical study that reproduces mass variations in the NW drainage system of GrIS and in entire Greenland. Information provided is similar to that reported in Table 1. Units are cm EWH (except for the linear trend and acceleration).

Region considered	NW	Entire Greenland
True signal	Eq. (17)	Eq. (18)
Random noise SD before regularization (true)	3.4	1.0
Random noise SD before regularization (VCE-based estimation)	3.30 ± 0.10	0.90 ± 0.08
Noise SD after regularization	1.29 ± 0.18	0.69 ± 0.05
Noise after regularization (% of original noise)	38	69
Bias in the linear trend (cm/yr)	0.00 ± 0.09	-0.02 ± 0.03
Bias in the acceleration signal (cm/yr ²)	0.01 ± 0.07	-0.01 ± 0.02
Bias in the "normal" annual signal (A_n)	N/A	-0.04 ± 0.13
Bias in the annual signal in 2012 (A_{2012})	N/A	0.44 ± 0.29

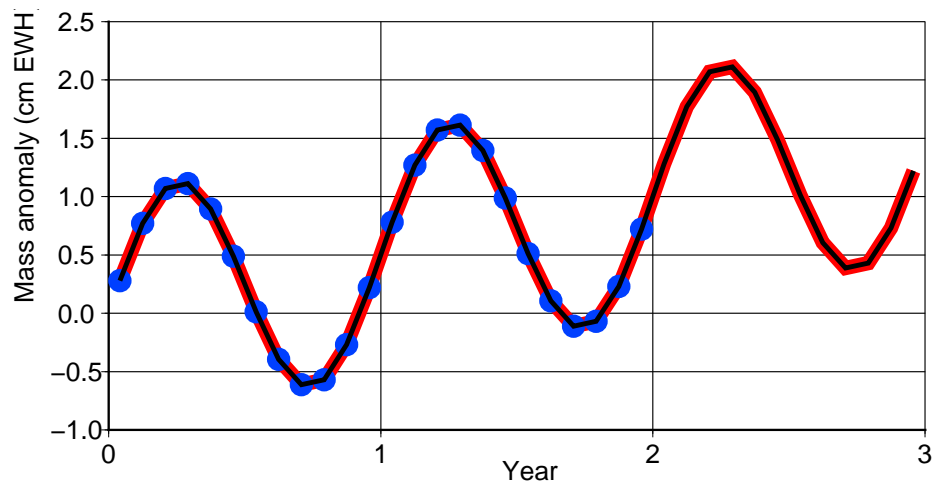


Figure 1: Simulated noiseless observations of mass anomalies (blue dots) and the time-series recovered on their basis with the proposed regularization technique (black line). The "true" time-series is shown in red.

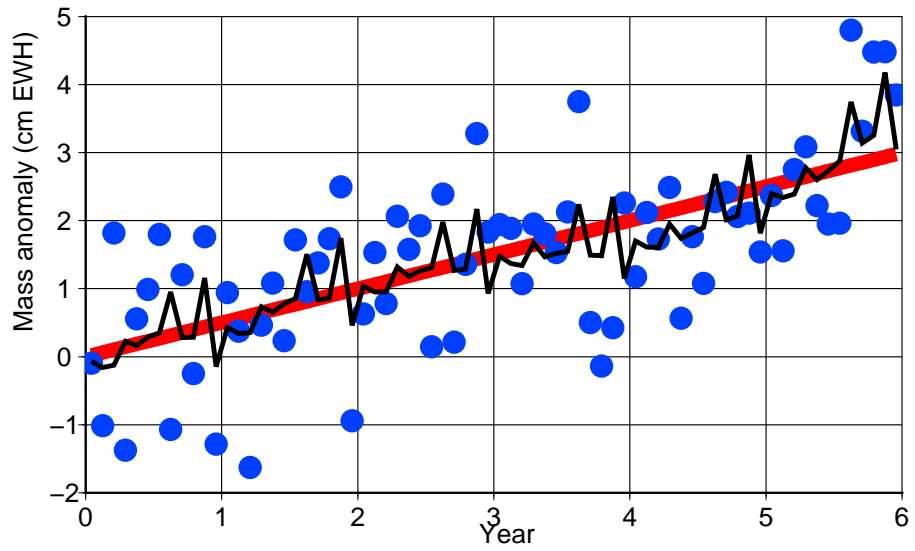
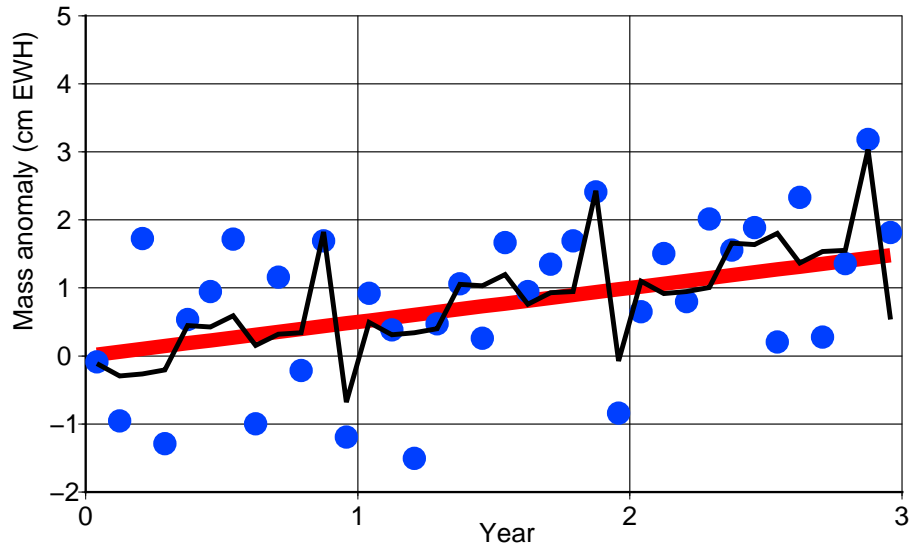


Figure 2: Simulated noisy observations of mass anomalies (blue dots) and the regularized time-series computed on their basis with the proposed technique (black line). The "true" time-series in shown in red. The considered time intervals are 3 year (top plot) and 6 years (bottom plot).

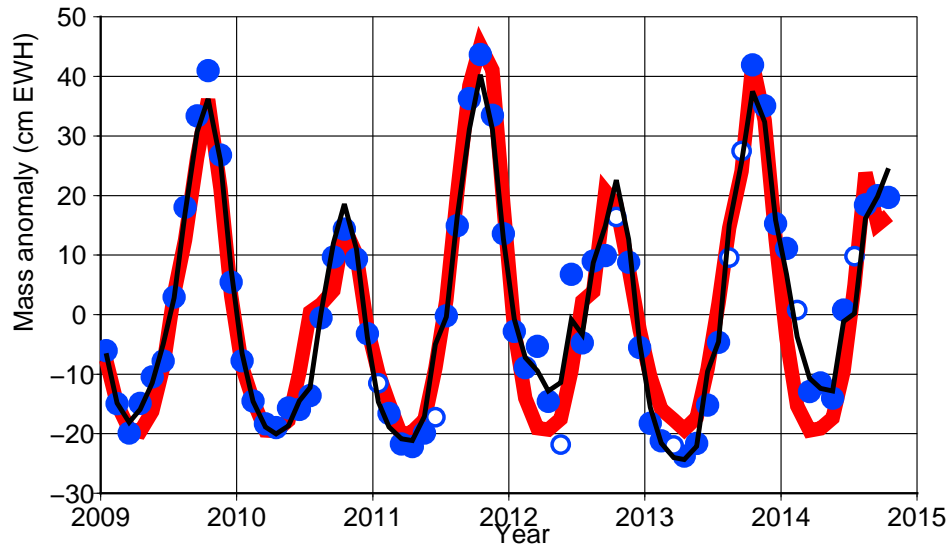
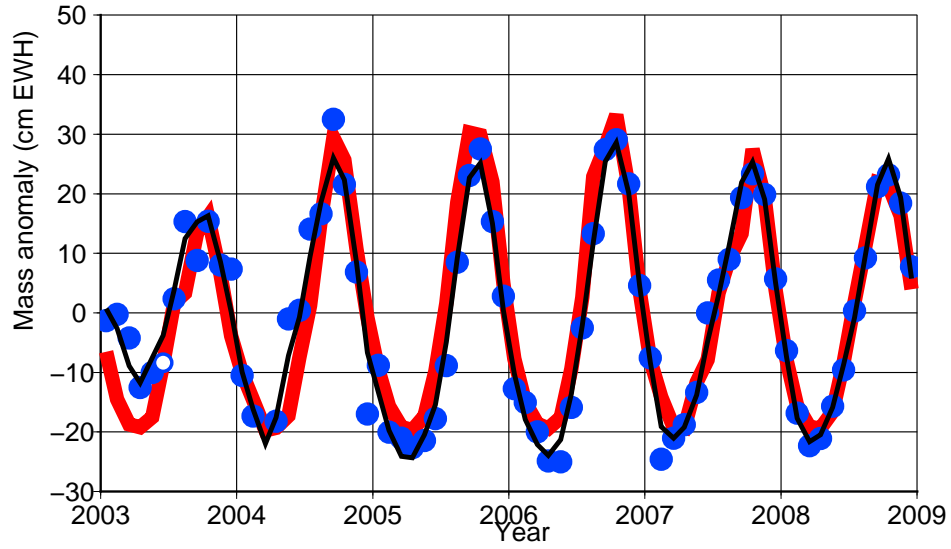


Figure 3: Mass anomalies at the Tonlé Sap basin: directly extracted from GRACE data without a regularization (blue circles) and obtained on their basis by cubic interpolation (open circles), as well as those obtained after applying the proposed regularization procedure (black line). Reference mass anomaly estimates based on MODIS data are shown in red. To make the illustration better readable, the entire time interval under consideration is split into two parts: 2003 – 2008 (top plot) and 2009 – 2014 (bottom plot).

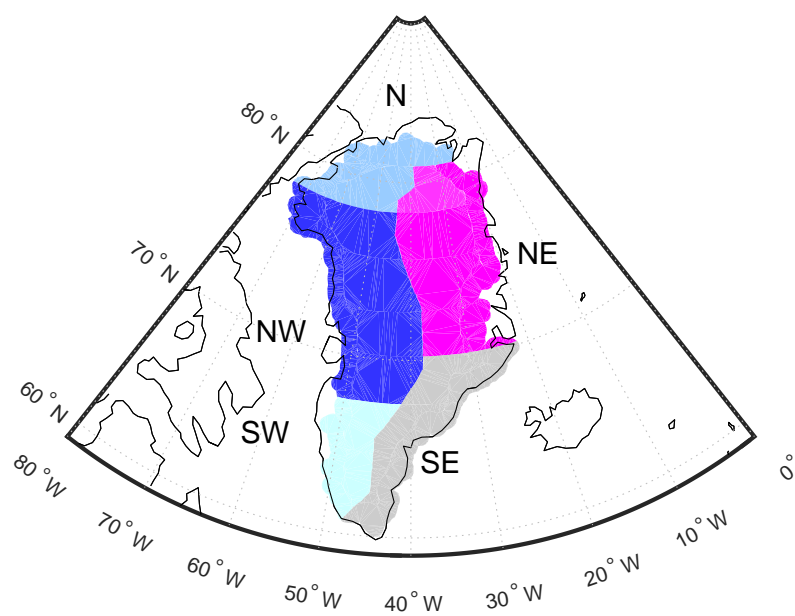


Figure 4: Adopted division of the territory of Greenland into individual drainage systems.

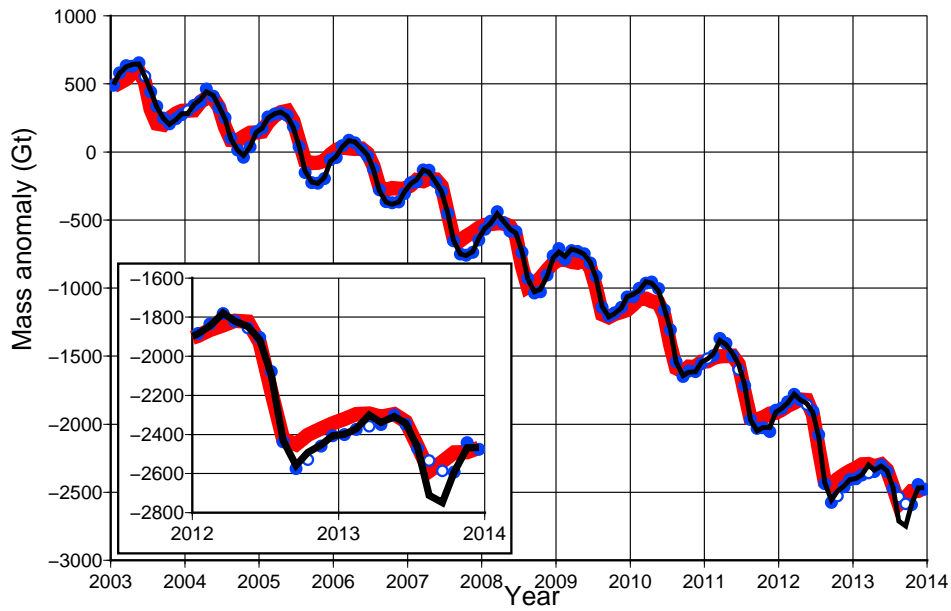
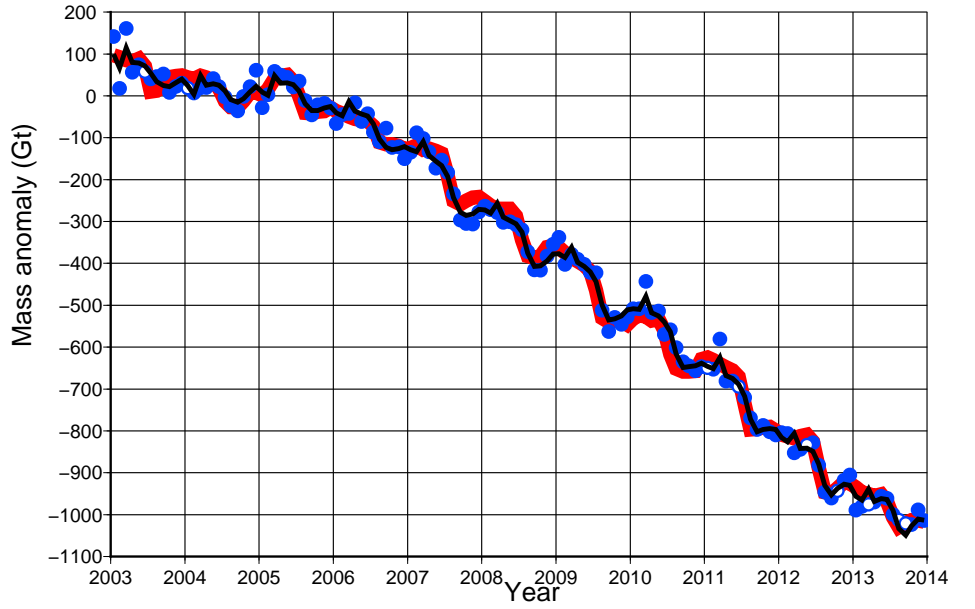


Figure 5: Mass anomalies in the NW drainage system (top plot) and entire Greenland (bottom plot). The plots show mass anomalies directly extracted from GRACE data without a regularization (blue circles) and obtained on their basis by cubic interpolation (open circles); as well as those obtained after applying the proposed regularization procedure (black line). Reference mass anomalies estimated on the basis of RACMO2.3 model are shown in red. The inset in the bottom plot zooms in on the time interval 2012 – 2013.

807 **Appendix A. Regularization of the discrete time-series and the optimal choice of the regu-**
 808 **larization parameter using Variance Component Estimation**

809 The description of Variance Component Estimation (VCE) is adapted from (Koch and Kusche,
 810 2002). We present VCE in the context of an arbitrary linear functional model, i.e. the model that
 811 links the data vector \mathbf{d} and the vector of unknown parameters \mathbf{x} with linear observation equations

$$\mathbf{Ax} = \mathbf{d}, \quad (\text{A.1})$$

812 where \mathbf{A} is an arbitrary matrix (frequently called "design matrix"). In our special case, matrix \mathbf{A}
 813 is unit.

814 The data can be contaminated by arbitrary correlated Gaussian noise. The noise covariance
 815 matrix \mathbf{C} is assumed to be known up to a scaling factor, i.e., it can be represented as

$$\mathbf{C} = \sigma_d^2 \mathbf{P}^{-1}, \quad (\text{A.2})$$

816 where \mathbf{P} is a known matrix (called "weight matrix") and σ_d^2 is an unknown constant.

817 The system Eq. (A.1) is to be solved under soft constraints, which are introduced by means of
 818 an additional set of linear equations

$$\mathbf{Dx} = \mathbf{0}, \quad (\text{A.3})$$

819 where \mathbf{D} is an arbitrary matrix. For instance, setting the matrix \mathbf{D} to the unit one reduces the
 820 soft constraints to the classical zero-order Tikhonov regularization. In our special case, matrix
 821 \mathbf{D} is defined such that the expression \mathbf{Dx} is the finite-difference analog of the double-difference
 822 expression $h'_{k+1}(t) - h'_k(t)$, cf. Eq. (5). This means that all the non-zero elements of matrix \mathbf{D} are
 823 equal, up to a constant scaling factor, to 1 or -1 . To prevent a jump at the beginning of each
 824 year, we apply the similar constraints also onto "December-January" pairs of months, i.e. by
 825 definition $x_{(k+1,1)} = x_{(k,13)}$, where the first lower index stands for the year and the second one for
 826 the calendar month of a year.

827 The set of soft constraints given by Eq. (A.3) can be interpreted as a system of additional
 828 observation equations with zero "observations" in the right-hand side. In what follows, those
 829 "observations" are called pseudo-observations.

830 Assuming that the pseudo-observations are contaminated by white noise, one can find the
 831 least-squares solution $\hat{\mathbf{x}}$ of the combined system composed of linear equations (A.1) and (A.3)
 832 by minimizing the penalty function

$$\Phi[\mathbf{x}] = \frac{1}{\sigma_d^2} (\mathbf{d} - \mathbf{Ax})^T \mathbf{P} (\mathbf{d} - \mathbf{Ax}) + \frac{1}{\sigma_x^2} \mathbf{x}^T \mathbf{Rx}, \quad (\text{A.4})$$

833 where σ_x^2 is the error variance of the pseudo-observations and \mathbf{R} is the regularization matrix,
 834 which is defined as

$$\mathbf{R} = \mathbf{D}^T \mathbf{D}. \quad (\text{A.5})$$

835 The multiplication of the penalty function (A.4) with σ_d^2 yields the equivalent penalty function

$$\tilde{\Phi}[\mathbf{x}] = (\mathbf{d} - \mathbf{Ax})^T \mathbf{P} (\mathbf{d} - \mathbf{Ax}) + \alpha \mathbf{x}^T \mathbf{Rx}, \quad (\text{A.6})$$

836 where α is the regularization parameter defined as

$$\alpha = \frac{\sigma_d^2}{\sigma_x^2}. \quad (\text{A.7})$$

837

838

839 The penalty functional (1) introduced at the beginning of the article is a continuous analog of the
 840 penalty function (A.6), provided that matrix \mathbf{P} is unit.

841 Obviously, the explicit expression for the vector $\hat{\mathbf{x}}$ minimizing the penalty function (A.4) (and,
 842 therefore, the penalty function given by Eq. (A.6)) is:

$$\hat{\mathbf{x}} = \frac{1}{\sigma_d^2} \mathbf{N}^{-1} \mathbf{A}^T \mathbf{P} \mathbf{d}, \quad (\text{A.8})$$

843 where \mathbf{N} is the normal matrix defined as

$$\mathbf{N} = \mathbf{N}_d + \mathbf{N}_x \quad (\text{A.9})$$

844 with

$$\mathbf{N}_d = \frac{1}{\sigma_d^2} \mathbf{A}^T \mathbf{P} \mathbf{A} \quad (\text{A.10})$$

845 and

$$\mathbf{N}_x = \frac{1}{\sigma_x^2} \mathbf{R}. \quad (\text{A.11})$$

846 The goal of the VCE method is to estimate the level of noise in each input data set. In the
 847 context of actual data, this means that the scaling factor σ_d^2 is to be found. If data noise is
 848 assumed to be white, so that matrix \mathbf{P} is unit, this task reduces to the estimation of the noise
 849 variance. Furthermore, both the actual observations and the pseudo-observations are treated by
 850 the VCE method equally. Since noise in pseudo-observations is assumed to be white, the VCE
 851 method can estimate the noise variance σ_x^2 of the pseudo-observations as well.

852 The VCE method is iterative. It starts from certain initial values $(\hat{\sigma}_d^2)_0$ and $(\hat{\sigma}_x^2)_0$, which allow
 853 the initial solution $\hat{\mathbf{x}}_0$ to be found with Eqs. (A.8 – A.11). Then, an updated estimate of factor σ_d^2
 854 is found as

$$\hat{\sigma}_d^2 = \frac{1}{n - \hat{\tau}_d} (\mathbf{d} - \mathbf{A}\hat{\mathbf{x}})^T \mathbf{P} (\mathbf{d} - \mathbf{A}\hat{\mathbf{x}}), \quad (\text{A.12})$$

855 where n is the number of data (i.e., the length of the vector \mathbf{d}) and

$$\hat{\tau}_d = \text{trace} [\hat{\mathbf{N}}_d \hat{\mathbf{N}}^{-1}]. \quad (\text{A.13})$$

856 The noise variance of pseudo-observations – factor σ_x^2 – is estimated similarly:

$$\hat{\sigma}_x^2 = \frac{1}{m - \hat{\tau}_x} \hat{\mathbf{x}}^T \mathbf{R} \hat{\mathbf{x}}, \quad (\text{A.14})$$

857 where m is the number of pseudo-observations (i.e., the length of the zero vector in the right-hand
 858 side of Eq. (A.3)) and

$$\hat{\tau}_x = \text{trace} [\hat{\mathbf{N}}_x \hat{\mathbf{N}}^{-1}]. \quad (\text{A.15})$$

859 The improved estimates of the factors σ_d^2 and σ_x^2 are used for an improved estimate of the solution
 860 \mathbf{x} , etc. The iterations are repeated until convergence.

861 **Appendix B. Proof that any function not penalized by the proposed regularization is a com-**
862 **bination of seasonal variations and linear trend**

863 Let us demonstrate analytically that any function $H(t)$ not penalized by the regularization
864 functional from Eq. (5) is a combination of arbitrary seasonal variations and a linear trend. Let
865 function $H(t)$ in the first and second year be equal to arbitrary functions $h_1(t)$ and $h_2(t)$, re-
866 spectively. Obviously, function $H(t)$ escapes penalization if and only if $h'_2(t) = h'_1(t)$, i.e., if
867 $h_2(t) = h_1(t) + C_1$, where C_1 is an arbitrary constant. Since the time-series of mass anomalies
868 is a continuous function, $h_2(0) = h_1(1)$. Therefore, constant C_1 can be represented as $C_1 =$
869 $h_2(0) - h_1(0) = h_1(1) - h_1(0)$ or, alternatively, $C_1 = h_2(1) - h_1(1) = h_2(1) - h_2(0)$. Thus, constant
870 C_1 is nothing but the yearly mass change, which is equal in the first and the second year. In the
871 third year, a non-penalized function $H(t)$ must be equal to $h_3(t) = h_2(t) + C_2$, where the constant
872 C_2 can be defined, in line with the derivation above, as $C_2 = h_3(1) - h_3(0) = h_2(1) - h_2(0) = C_1$.
873 Therefore, $h_3(t) = h_1(t) + 2C_1$. By considering the further years, we readily find that function
874 $H(t)$ avoids penalization if it is defined in the k -th year as

$$h_k(t) = h_1(t) + (k - 1) C_1. \quad (\text{B.1})$$

875 The first term in Eq. (B.1) describes an arbitrary seasonal variability; the second term is a linear
876 function of time and represents a long-term linear trend.